Creating drag and lift curves from soccer trajectories

GOFF, John, KELLEY, John <http://orcid.org/0000-0001-5000-1763>, HOBSON, Chad, SEO, Kazuya, ASAI, Takeshi and CHOPPIN, Simon <http://orcid.org/0000-0003-2111-7710>

Published version

GOFF, John, KELLEY, John, HOBSON, Chad, SEO, Kazuya, ASAI, Takeshi and CHOPPIN, Simon (2017). Creating drag and lift curves from soccer trajectories. European Journal of Physics, 38 (4).

Creating drag and lift curves from soccer trajectories

J E Goff[1], J Kelley[2], C M Hobson[1], Kazuya Seo[3], Takeshi Asai[4] and S B Choppin[2]

[1] Lynchburg College, Lynchburg, Virginia 24501, USA

[2] Centre for Sports Engineering Research, Sheffield Hallam University, Sheffield, UK

[3] Faculty of Education, Art and Science,Yamagata University, 1-4-12 Kojirakawa, Yamagata 990-8560, Japan

[4] Inst. of Health and Sports Sci., Comprehensive Human Sciences University of Tsukuba, Tsukuba, 305-8574, Japan.

E-mail: s.choppin@shu.ac.uk

Abstract. Trajectory analysis is an alternative to using wind tunnels to measure a soccer balls aerodynamic properties. It has advantages over wind tunnel testing such as being more representative of game play. However, previous work has not presented a method that produces complete, speed -dependent drag and lift coefficients. Four high-speed cameras in stereo-calibrated pairs were used to measure the spatial co-ordinates for 29 separate soccer trajectories. Those trajectories span a range of launch speeds from 9.3 m/s to 29.9 m/s. That range encompasses low-speed laminar flow of air over a soccer ball, through the drag crises where air flow is both laminar and turbulent, and up to high-speed turbulent air flow. Results from trajectory analysis were combined to give speed-dependent drag and lift coefficient curves for the entire range of speeds found in the 29 trajectories. Average root mean square error between measured and modelled trajectory was 0.028 m horizontally and 0.034 m vertically. The drag and lift crises can be observed in the plots of drag and lift coefficients respectively.

PACS numbers: 01.80.+b, 45.10.-b, 47.11.-j, 47.85.Gj

Keywords:aerodynamics, drag, football, sport, soccer, trajectory analysis

Submitted to: *Eur. J. Phys.*

1. Introduction

Association football, or soccer, is a sport that continually evolves – the World Cup sees a new ball every four years. Though the international governing body, FIFA, controls the weight, size and sphericity of the ball, rules for soccer allow balls with different panel numbers, seam shapes, groove depths, and surface textures. The aerodynamic characteristics accompanying each new ball have lead to controversy in the past. Perceived differences in flight behaviour and criticism from players highlights the importance of aerodynamic testing and assessment.

The most common way of measuring a soccer ball's aerodynamic properties is with a wind tunnel. Much of the recent work has been summarized in a 2013 review article [1], but we will adumbrate pertinent work here, including work published since the aforementioned review article.

One research group [2] measured the drag coefficients of three types of soccer balls that were set spinning in their wind tunnel. They experimented past the drag crisis, where laminar flow turns to turbulent flow at increased speeds [3], and found that a tripling of the spin parameter resulted in an approximate doubling of the drag coefficient.

Other wind-tunnel researchers using small-scale balls [4] and regulation-sized balls [5] found in their wind-tunnel studies that a reverse Magnus effect, also seen in cricket [6], was possible for speeds below the drag crisis and for small spin parameters. Researchers [7, 8, 9, 10, 11, 12, 13] have also used wind tunnels to study the influence of ball surface on aerodynamics. Balls with little to no spin, giving rise to so-called knuckle effects, have been investigated [14, 15, 16, 17], too.

Wind tunnels are natural devices for studying soccer ball aerodynamics because they move air across a ball while sensors measure the magnitude and direction of force. Wind tunnels, however, cannot completely simulate a ball moving through air because the ball must be mounted in place and the air flow must have constant speed and direction. The ball is held in place using a rod typically mounted on the downstream side of the ball [18, 19]. This can have some effect on the flow of air around the ball, meaning the rod influences the aerodynamic coefficients extracted from wind-tunnel measurements. If researchers wish to spin the ball, the rod must be attached to the side of the ball which can have much larger effects on the flow of air around the ball.

Trajectory analysis is a method for studying soccer balls in environments more representative of game play than those provided by wind tunnels. It is also an attractive option for researchers who may have budget and interior space limitations that make it impossible to acquire and experiment with a wind tunnel. In trajectory analysis, a moving ball, usually projected from a machine or kicked by a player, is tracked using optical [1, 20] or radar-based [21] sensors. The spatial co-ordinates are analysed to calculate the aerodynamic characteristics of the ball.

Wind tunnels do have a few advantages over trajectory analysis. Unless one is in possession of a high-quality ball-firing machine, using trajectory analysis to experiment with specific ball speeds and spin rates is more difficult than using the controlled environments of wind tunnels. In a wind-tunnel, aerodynamic coefficients are obtained from time-averaged

forces measured during a steady-state conditions. In trajectory analysis coefficients are extracted from data recorded during unsteady flight (the ball is under constant deceleration) and authors have noted this difference [22].

Research work employing trajectory analysis utilizes physics [23, 24] to explore dominant interactions between air and ball [25]. Researchers have used trajectory analysis methods to extract information on boundary-layer separation [26, 27]. An early attempt [28] at trajectory analysis of soccer balls in flight used quadratic-time functions for data smoothing, but such functions are good only for constant-acceleration motion – in football flight, acceleration varies with time. Both free kicks [29, 30] and corner kicks [30] have been modelled with trajectory analysis. Wind-tunnel methods and trajectory analysis were recently combined [31] to show the increased aerodynamic stability of the Brazuca over the Jabulani. The former ball was used in the 2014 World Cup in Brazil, whereas the latter ball was used in the 2010 World Cup in South Africa.

In this present study we build upon trajectory analysis work [32, 33] that established methods for extracting drag and lift coefficients in both two and three dimensions. That previous work revealed lift coefficients for spin parameters inaccessible by wind tunnels. We also expand upon recent work [20] that described an approach to recreate drag profiles from multiple soccer trajectories. By studying trajectories below, within, and above the drag crisis, we use and expand upon the techniques referenced in this paragraph to create drag and lift curves as functions of speed. We thus create a full aerodynamic profile for the ball used in our experiments.

2. Methods

2.1. Trajectory data collection

We used a standard pattern 32-panel Puma League soccer ball with mass $m = 0.424\,\mathrm{kg}$. The ball was projected using a ball launcher that uses rotating disks which also allow spin to be imparted onto the ball.

Four frame-locked, high-speed video cameras (Phantom V4, Vision Research, USA) running at 200 frames per second were used to obtain 3D ball positions throughout each trajectory. The cameras were arranged as two pairs, with each camera positioned as in Figure 1. One pair of cameras was focused on the first half of the trajectory and the second pair was focused on the second half of the trajectory. Each camera pair was calibrated independently using a planar checker-board technique. The intrinsic camera parameters were measured using the planar calibration technique developed by Zhang [34]. Software that facilitates stereo calibration is freely available as a MATLAB toolbox [35] and stand-alone software, Check3D [36]. To calibrate each camera-pair a checker-board (1 m by 0.5 m) was moved into 30 different positions which 'filled' the calibration volume. The board was visible by both cameras at each position and the resulting camera images were used in the calibration software.

The co-ordinate systems of both pairs were aligned using an orthogonal axes alignment

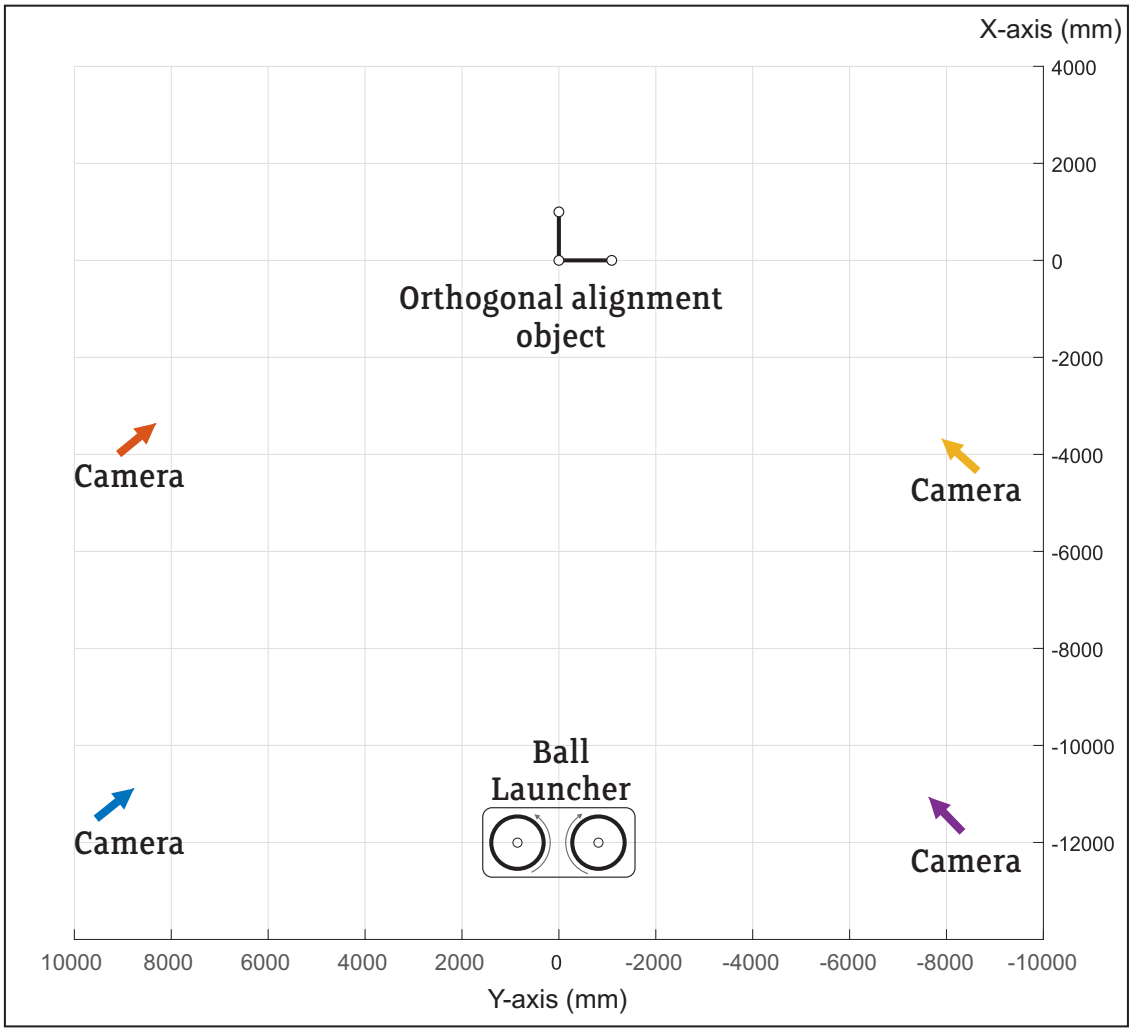

Figure 1. A plan of the camera and ball launcher locations relative to the axes alignment object position (units in mm)

object placed in the region indicated in Figure 1. The x-axis was aligned to the horizontal directly away from the ball launcher, the y-axis was aligned to the horizontal perpendicular to the x-axis and the z-axis was aligned to the vertical. The 3D position of a launched ball could be calculated provided it was visible in the frames of both cameras of a single camera pair. This technique resulted in a calibrated region approximately 18 metres in length, allowing large trajectories to be analysed.

Ball centres were manually digitised from each camera frame and converted into 3D co-ordinates aligned to the orthogonal alignment object. Each trajectory essentially stayed within a single 2-dimensional plane but they were not always parallel to the global x-axis due to small deviations launch angle. Trajectories were re-aligned using principle component analysis such that the new x-component was distance from the launcher, the z-component was the height and the y-component was zero throughout.

Angular speed, ω, was found by stepping through each trajectory film and following a given marking on the ball. Filming from the side meant we could not ascertain the fraction

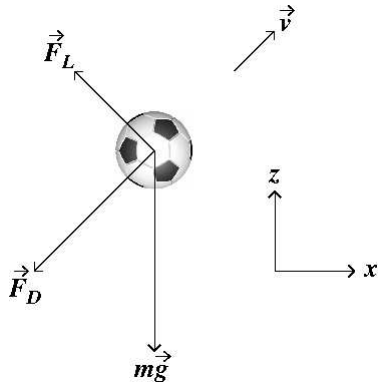

Figure 2. Forces acting on a soccer ball moving with velocity $\vec{v}$. Shown, too, is the x-z Cartesian coordinate system

of spin that was pure topspin. That means we may have overestimated the component of spin contributing to topspin.

Uncertainties associated with this method arise from digitisation error and from camera pair alignment (which incorporate camera calibration uncertainties). The largest uncertainties were found from camera alignment. Comparing the 3-dimensional reconstruction of points from both camera pairs across a 4-m overlapping region showed a maximum difference of 50 mm. The errors due to digitisation were highest when the ball was furthest from the camera, at which point each pixel represented 10 mm. Spatial resolution was lower than this as the digitisation software allowed for sub-pixel selection – a conservative estimate is 5 mm.

2.2. Drag and lift coefficient equations

The aligned trajectories were planar and used the x-z Cartesian coordinate system as shown in Figure. 2. The ball's weight was $mg = 4.156\,\mathrm{N}$, where $g = 9.8\,\mathrm{m/s^2}$. Buoyancy forces were ignored, as these were just 1.3% of the ball's weight. The air exerted a single force on the ball, but we split that force into components traditionally seen in fluid mechanics [37]. The drag force was in the direction opposite the ball's velocity, $\vec{v}$, and had magnitude

$$F_D = \frac{1}{2}\rho A v^2 C_D\,, \tag{1}$$

where $\rho = 1.2\,\mathrm{kg/m^3}$ was the air density, $A \simeq 0.0333\,\mathrm{m^2}$ was the ball's cross-sectional area, $v = |\vec{v}|$ was the ball's speed, and C_D was the dimensionless drag coefficient that depended on the ball's speed and spin rate. Orthogonal to the drag force was the lift force, which had magnitude

$$F_L = \frac{1}{2}\rho A v^2 |C_L|\,, \tag{2}$$

where C_L was the dimensionless lift coefficient which also depended on the ball's speed and spin rate. The direction of the lift force shown in Figure. 2 represents $C_L > 0$ and usually means the ball has backspin.

Newton's second law gives the soccer ball's equation of motion as

$$m\vec{a} = \vec{F}_D + \vec{F}_L + m\vec{g}, \tag{3}$$

where $\vec{a}$ is the ball's acceleration while in flight.

Using the Cartesian coordinate system shown in Figure. 2, Eq. 3 may be split into x and z components as [32]

$$a_x = -\beta\, v\, (C_D\, v_x + C_L\, v_z) \tag{4}$$

and

$$a_z = \beta\, v\, (-C_D\, v_z + C_L\, v_x) - g, \tag{5}$$

where $\beta = \rho A/2m \simeq 0.0471\,\mathrm{m}^{-1}$.

As has been described elsewhere [32], Eqs. 4 and 5 may be solved for C_D and C_L, giving

$$C_D = -\left[\frac{(a_z+g)\, v_z + a_x\, v_x}{\beta\, v^3}\right] \tag{6}$$

and

$$C_L = \frac{(a_z+g)\, v_x - a_x\, v_z}{\beta\, v^3}. \tag{7}$$

Note that here, $v = \left(v_x^2 + v_z^2\right)^{1/2}$.

2.3. Trajectory smoothing

This approach takes coordinates from a trajectory, numerically determines the velocity and acceleration components, and uses Eqs. 6 and 7 to find C_D and C_L, respectively. One challenge of this approach is that numerical derivatives of trajectory data are prone to large errors. Errors in digitisation are amplified through derivation and the numerical algorithms also introduce error. This challenge is met by smoothing trajectory data, typically by fitting the x and z coordinates to polynomials in time. Evaluating derivatives of polynomials analytically allows one to find C_D and C_L as functions of v from Eqs. 6 and 7. The order of the polynomials should be chosen such that the data is explained without over-fitting the data. In this case, 3^{rd} order polynomials were chosen. Orders higher than this showed symptoms of over-fitting, whilst orders lower than 3 would force the fitted trajectory to have a constant acceleration.

Polynomials were fitted to each of the 29 trajectories. Eqs. 6 and 7 were then used to calculate C_D and C_L at each point in time for which there was a measured ball position. This ensured that the weighting of the points used to create the C_D and C_L curves matched the collected data. Fifth order polynomials were chosen to fit the C_D against velocity and C_L against velocity data. These polynomials provided our C_D and C_L curves.

2.4. Wind-tunnel comparison

For purposes of comparison, the aerodynamic profile of the ball was measured using a low-speed, circulating wind tunnel with a six-component balance (maximum wind velocity = 40ms[1]; measuring section = 1.5 1 m; turbulence level = 1%) at the Department of Aeronautics

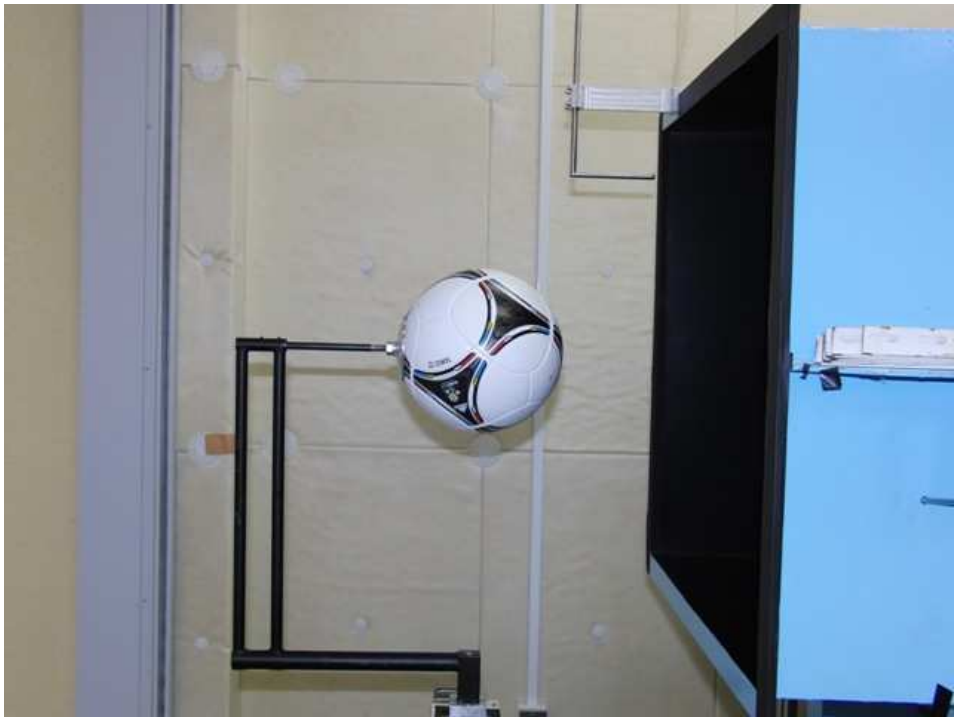

Figure 3. The wind tunnel setup. The ball was supported at the rear by a sting

& Astronautics, Tokai University, Japan. During testing the ball had no spin and was secured at the rear by a sting which was attached to the force balance as shown in figure 3. Wind speeds were increased from 7 ms^{-1} to 35 ms^{-1} in approximate 1 ms^{-1} intervals. The resulting forces were measured and converted to drag coefficient using Eqs 1 and 2.

3. Results

Table 1 summarises the 29 trajectories including launch conditions and spin information. Depending on ball velocity, a point on the ball could be followed by as much as a complete ball revolution, or as little as only a quarter of a ball revolution. This will have introduced some uncertainty. However the methods presented here for determining the drag and lift profiles do not use the angular velocity of the ball. Because an appreciable fraction of a trajectory must be viewed to find ω, we refer to the time-averaged angular speed in Table 1, where $< \cdots >$ represents time average. We also determine the time-averaged spin parameter, given by [37]

$$\mathrm{Sp} = \frac{r\,\omega}{v}\,, \tag{8}$$

where average values of ω and v are used in Eq. 8. Average speeds are taken from the numerically-determined trajectories in Figure. 6.

The method resulted in between 46 and 112 C_D and C_L values per trajectory, each with an associated velocity value. In total, there were 2022 points and these are shown with the fitted C_D and C_L curves in Figure 4 and Figure 5. Trajectories 22 and 24 were omitted from the data used to fit the C_D and C_L curves because the C_D value changed drastically throughout

Table 1. Trajectory Information: Initial velocity, mean velocity, initial Reynolds number, launch angle, mean angular velocity (topspin) and spin parameter, where $< \cdots >$ represents time average

Trajectory	v_0 (m/s)	$\mathrm{Re}_0 \times 10^{-5}$	θ_0 (rad)	$< v >$ (m/s)	$< \omega >$ (rad/s)	$< Sp >$
1	29.83	3.99	0.105	27.12	17.45	0.066
2	29.93	4.00	0.106	27.04	21.69	0.083
3	29.72	3.98	0.115	26.98	17.97	0.069
4	29.45	3.94	0.084	26.91	27.70	0.106
5	27.39	3.66	0.121	24.68	26.75	0.112
6	26.65	3.56	0.084	24.49	28.80	0.121
7	26.96	3.61	0.098	24.74	24.17	0.101
8	27.21	3.64	0.119	24.53	20.65	0.087
9	23.89	3.20	0.134	21.71	18.91	0.090
10	23.74	3.17	0.143	21.53	25.17	0.120
11	23.67	3.17	0.131	21.73	19.37	0.092
12	20.63	2.76	0.153	18.79	14.68	0.080
13	20.51	2.74	0.117	18.94	21.24	0.115
14	20.60	2.75	0.096	19.28	23.72	0.127
15	20.46	2.74	0.142	18.72	16.34	0.090
16	17.28	2.31	0.117	16.34	12.89	0.081
17	17.33	2.32	0.080	16.51	17.95	0.112
18	17.12	2.29	0.161	16.15	12.59	0.080
19	17.30	2.31	0.063	16.44	15.54	0.097
20	11.39	1.52	-0.066	11.94	17.58	0.152
21	12.13	1.62	-0.012	12.34	10.95	0.091
22	11.56	1.55	-0.004	12.07	14.16	0.121
23	9.69	1.30	0.066	9.65	10.22	0.109
24	9.30	1.24	0.050	9.38	8.67	0.095
25	9.79	1.31	0.056	9.67	11.86	0.126
26	9.67	1.29	0.084	9.57	10.95	0.118
27	10.79	1.44	0.356	9.79	10.30	0.108
28	10.70	1.43	0.380	9.65	9.18	0.098
29	10.84	1.45	0.358	9.84	11.52	0.121

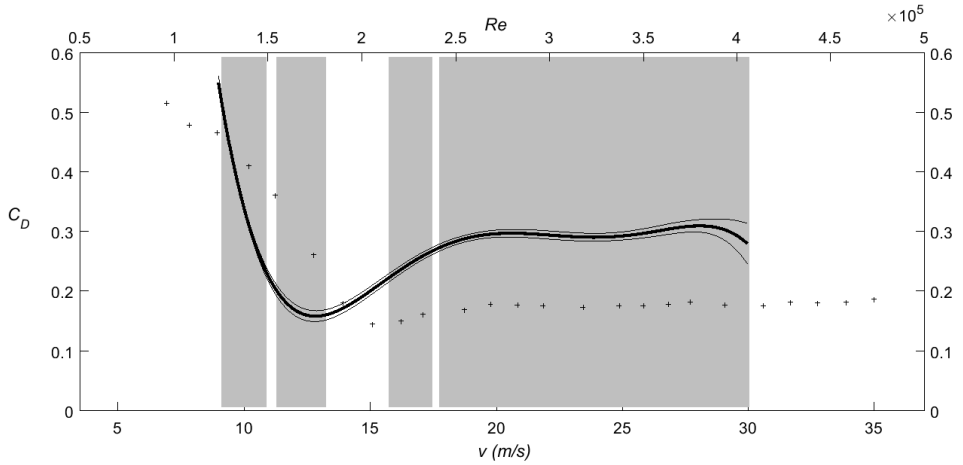

Figure 4. An order 5 polynomial with 99% curve prediction intervals fitted to the all of the C_D - velocity points from all of the trajectories. Trajectories 22 and 24 were omitted. The grey regions show the velocities spanned by the trajectories. Wind tunnel data is shown as black crosses.

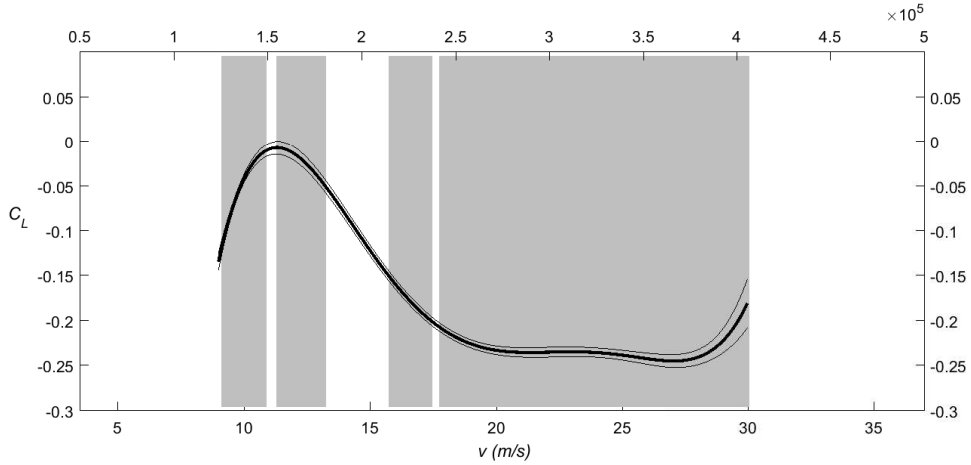

Figure 5. An order 5 polynomial with 99% curve prediction intervals fitted to the all of the C_L - velocity points from all of the trajectories. Trajectories 22 and 24 were omitted. The grey regions show the velocities spanned by the trajectories.

both fitted trajectories. For trajectory 22, the C_D was also negative for half of the trajectory. This suggests that the fitted trajectories were not correct.

The coefficients for the C_D and C_L curves are shown in Table 2 such that the C_D curve is given by

$$C_D(v) = \sum_{j=0}^{5} \delta_j v^j \tag{9}$$

Table 2. Fitting Coefficients for Eqs. 9 and 10

C_D	C_L
$\delta_0 = 14.276$	$\lambda_0 = -9.448$
$\delta_1 = -3.730\,\mathrm{s/m}$	$\lambda_1 = 2.675\,\mathrm{s/m}$
$\delta_2 = 3.801 \times 10^{-1}\,(\mathrm{s/m})^3$	$\lambda_2 = -2.885 \times 10^{-1}\,(\mathrm{s/m})^3$
$\delta_3 = -1.873 \times 10^{-2}\,(\mathrm{s/m})^3$	$\lambda_3 = 1.482 \times 10^{-2}\,(\mathrm{s/m})^3$
$\delta_4 = 4.487 \times 10^{-4}\,(\mathrm{s/m})^4$	$\lambda_4 = -3.681 \times 10^{-4}\,(\mathrm{s/m})^4$
$\delta_5 = -4.201 \times 10^{-6}\,(\mathrm{s/m})^5$	$\lambda_5 = 3.561 \times 10^{-6}\,(\mathrm{s/m})^5$

and the C_L curve is given by

$$C_L(v) = \sum_{j=0}^{5} \lambda_j v^j \,. \tag{10}$$

In Figure. 4 the drag crisis is shown to be around $v = 12.5\,\mathrm{m/s}$, $\mathrm{Re} = 1.7 \times 10^5$ for the trajectory testing and $v = 15\,\mathrm{m/s}$, $\mathrm{Re} = 2.00 \times 10^5$ for wind-tunnel testing. Post-critical C_D values are higher in the trajectory testing results than those measured in a wind-tunnel. After the drag crisis, the trajectory testing C_D values initially increase and then remain unchanged as velocity increases. Wind-tunnel C_D values do not increase with velocity after the drag crisis, and so are below the 99% prediction curve for the fitted trajectory testing C_D values. The spin parameter, Sp, was approximately 0.1 for all trajectories. Therefore the post drag-crisis values of C_L seen in Figure. 5 are consistent with what has been measured for a spinning ball with Sp close to 0.1 in a wind tunnel [2] and using trajectory analysis [33].

Equipped with Eqs. 9 and 10 and each trajectory's initial conditions given in Table 1, we numerically solved Eq. 3 for each trajectory. We show in Figure 6 a representative sample of the numerically-determined trajectories with their corresponding real trajectories. We note remarkable agreement between trajectories created from our speed-dependent C_D and C_L functions and the actual trajectories.

To quantify the agreement with the real trajectories, the Root Mean Square Error (RMSE) was calculated for each numerically-determined trajectory. The mean RMSE for the horizontal components was 0.028 m, with the maximum being 0.084 m. The mean RMSE for the vertical components was 0.034 m, with the maximum being 0.077 m.

4. Discussion

We have used football trajectories repeated at a number of launch speeds and angles to derive the aerodynamic profiles of a football. While the methods used are not new [22, 38, 27] , this is the first time the technique has been at this scale and range of speeds. As a result we have been able to calculate the drag and lift of our ball at transitional and post-critical Reynolds numbers.

The coefficient of drag values derived from trajectories are different to those obtained in wind-tunnel testing. Transition occurs sooner and post-critical drag is higher. The balls

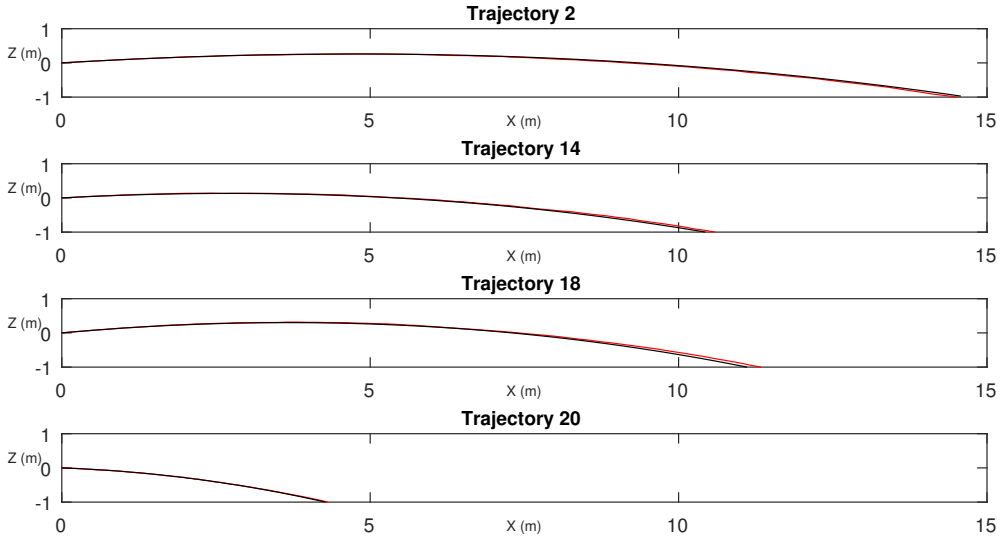

Figure 6. Plots of a representative sample of the trajectories. The red lines show the polynomial fitted to the measured position and the black lines show the trajectories calculated using the launch conditions and the C_D and C_L curves.

we tested were all spinning – which can increase the coefficients of drag. However, the magnitudes of spin we measured do not account for the differences in C_D we observed according to published data [5, 2]. Other authors have noted similar differences between the wind-tunnel and trajectory testing [22]. These have been attributed to the inherent unsteady nature of ball flight compared to the steady-state conditions created in a wind-tunnel. In other areas of wind-tunnel use, cycling for example, the assumption of steady-state is valid because the rider is able to generate power to equalise the retarding forces of air resistance. This is not possible in a ball's free-flight.

This brings us to a dichotomy. The wind-tunnel is the only tool available (leaving computer simulation aside) to test and compare ball designs in a precise and controlled environment. However, trajectory analysis provides the means to assess the performance of sports balls in realistic conditions where it is easier to create ball spin and the effects of ball supports do not have to be accounted for.

In our study, the ball was spinning upon launch but this spin was not constant (Table 1). It was necessary to add spin to the ball because our launching equipment was not able to produce a consistent trajectory in the non-spin condition. While spin was set to the lowest setting, it increased with ball speed due to the increasing speed of the launcher's wheels. The increasing ball spin resulted in a relatively stable spin parameter (0.10 on average) which has a weak, negative correlation with ball speed (Pearson's $r = -0.42$).

Previous research which has examined football lift coefficient has reported positive relationships with both ball speed (at constant spin) [5] and spin parameter (at constant speed) [2].

In our study, the largest magnitudes of lift coefficient are reported for the highest ball

speeds but a crisis in lift coefficient is visible at the critical Reynolds number (around 1.5×10^5 5). In this region lift collapses to zero. The lift-crisis or reverse-magnus effect is well known, has been reported and investigated by others [39, 40] and shown to occur in rotating spheres at around the critical Reynolds number [41]. Around transition, turbulent and laminar flow regimes can exist on opposite sides of a spinning ball, reversing the direction of the magnus effect, or eliminating it altogether. Passmore et al. [5] observed reverse magnus effect at Reynolds numbers between 1.5×10^5 and 2.0×10^5 when testing footballs in a wind-tunnel but they did not test at Reynolds numbers below 1.5×10^5. Our study has calculated the lift coefficient at Reynolds numbers as low as 1.25×10^5 and shows a return to standard magnus effect.

This study has shown that it's possible to obtain full drag and lift profiles for a football through trajectory analysis, indicating transition and the lift-crisis. However, in order to do so, significant manual labour was required. This included manual digitisation in four separate camera views (for each recorded short) and a complex physical set-up. If studies of this type are to expand to include a large number of ball types, spins and speeds, advancements in the methods of data collection are required. Other authors have used light-gate arrays to precisely calculate ball position and time [38, 22] but this becomes impractical at the scale required for football analysis. A dedicated space, configured for automatic ball tracking and spin-detection is now feasible and would be ideal for future testing.

Trajectory testing is a feasible way to assess the real-world performance of football designs, giving drag and lift coefficients which could be reliably used to predict future behaviour. However, the practical requirements for assessments of this scale do not suggest it is a low-cost alternative to the wind-tunnel.

5. Conclusions

We have shown how to obtain full drag and lift curves as functions of velocity from trajectory analysis. These curves include transition between laminar and turbulent flow regimes and show the lift-crisis which occurs in spinning balls around transition.

Differences in drag values from wind-tunnel testing highlight the different natures of this type of testing - where there are unsteady states and a looser control in the parameters. Trajectory testing is more appropriate in predicting ball behaviour and trajectories. However, it lacks the precise control which is possible in the wind-tunnel.

The next step in this line of research is to explore large-scale, automated methods of obtaining ball trajectories with spin. This would allow researchers to analyse higher spin rates and more complex aerodynamic interactions.

Acknowledgments

acknowledgements We would like to thank Dr Nathan Elliott for his diligent work in digitisation.

6. References

[1] John Eric Goff. A review of recent research into aerodynamics of sport projectiles. *Sports Engineering*, 16(3):137–154, 2013.

[2] T Asai, K Seo, O Kobayashi, and R Sakashita. Fundamental Aerodynamics of the Soccer Ball. *Sports Engineering*, (10):101–110, 2007.

[3] R D Mehta. Aerodynamics of Sports Balls. *Annual Review of Fluid Mechanics*, 17(1):151–189, jan 1985.

[4] MJ Carré, S R Goodwill, and S J Haake. Understanding the Effect of Seams on the Aerodynamics of an Association Football. *Proceedings of the Institution of Mechanical Engineers, Part C: Journal of Mechanical Engineering Science*, 219(7):657–666, jul 2005.

[5] M A Passmore, S Tuplin, A Spencer, and R Jones. Experimental Studies of the Aerodynamics of Spinning and Stationary Footballs. *Journal of Mechanical Engineering Science*, 222:195–205, 2007.

[6] R D Mehta. An overview of cricket ball swing. *Sports Engineering*, 8(4):181–192, 2005.

[7] Firoz Alam, Harun Chowdhury, and Hazim Moria. A comparative study of football aerodynamics. In *Procedia Engineering*, volume 2, pages 2443–2448, Vienna, Austria, 2010. Elsevier.

[8] Firoz Alam, Harun Chowdhury, Hazim Moria, Franz Konstantin Fuss, Iftekhar Khan, Fayez Aldawi, and Aleksandar Subic. Aerodynamics of contemporary FIFA soccer balls. In *Procedia Engineering*, volume 13, pages 188–193, 2011.

[9] Takeshi Asai, Shinichiro Ito, Kazuya Seo, and Sekiya Koike. Characteristics of modern soccer balls. In *Procedia Engineering*, volume 34, pages 122–127, 2012.

[10] Firoz Alam, Harun Chowdhury, Mark Stemmer, Zilong Wang, and Jie Yang. Effects of surface structure on soccer ball aerodynamics. In *Procedia Engineering*, volume 34, pages 146–151, 2012.

[11] Thorsten Kray, Jörg Franke, and Wolfram Frank. Magnus effect on a rotating soccer ball at high Reynolds numbers. *Journal of Wind Engineering and Industrial Aerodynamics*, 124:46–53, 2014.

[12] Takeshi Asai and Kazuya Seo. Aerodynamic drag of modern soccer balls. *SpringerPlus*, 2:171, 2013.

[13] Sung Chan Hong and Takeshi Asai. Effect of panel shape of soccer ball on its flight characteristics. *Scientific Reports*, 4:7, 2014.

[14] Sungchan Hong, Chulsoo Chung, Masao Nakayama, and Takeshi Asai. Unsteady aerodynamic force on a knuckleball in soccer. In *Procedia Engineering*, volume 2, pages 2455–2460, 2010.

[15] Takeshi Asai and Kyoji Kamemoto. Flow structure of knuckling effect in footballs. *Journal of Fluids and Structures*, 27(5-6):727–733, 2011.

[16] Masahide Murakami, Kazuya Seo, Masakazu Kondoh, and Yutaka Iwai. Wind tunnel measurement and flow visualisation of soccer ball knuckle effect. *Sports Engineering*, 15(1):29–40, 2012.

[17] Shinichiro Ito, Masaharu Kamata, Takeshi Asai, and Kazuya Seo. Factors of unpredictable shots concerning new soccer balls. In *Procedia Engineering*, volume 34, pages 152–157, 2012.

[18] E Achenbach. Experiments on the flow past spheres at very high Reynolds numbers. *Journal of Fluid Mechanics*, 54:565–575, 1972.

[19] E Achenbach. The effects of surface roughness and tunnel blockage on the flow past spheres. *Journal of Fluid Mechanics*, 65:113–125, 1974.

[20] S B Choppin. Calculating football drag profiles from simulated trajectories. *Sports Engineering*, 16(3):189–194, jul 2013.

[21] David Rogers, Martin Passmore, Andy Harland, Roy Jones, Chris Holmes, and Tim Lucas. An experimental validation method of wind tunnel measurements on FIFA approved footballs using kicking tests in wind-free conditions. *Procedia Engineering*, 2(2):2481–2486, 2010.

[22] Yasufumi Konishi, Hiroyuki Okuizumi, and Tomoyuki Ohno. Piv measurement of a flying table tennis ball. *Procedia Engineering*, 147:104–109, 2016.

[23] Neville de Mestre. *The Mathematics of Projectiles in Sport*. Cambridge University Press, 1990.

[24] C White. *Projectile Dynamics in Sport: Principles and Applications*. 2010.

[25] T. G. Myers and S. L. Mitchell. A mathematical analysis of the motion of an in-flight soccer ball. *Sports Engineering*, 16(1):29–41, 2013.

[26] J. E. Goff, W. H. Smith, and M. J. Carré. Football boundary-layer separation via dust experiments. *Sports*

Engineering, 14(2-4):139–146, 2011.

[27] John Eric Goff and Matt J. Carré. Investigations into soccer aerodynamics via trajectory analysis and dust experiments. In *Procedia Engineering*, volume 34, pages 158–163, 2012.

[28] M J Carré, T Asai, T Akatsuka, and S J Haake. The curve kick of a football II: flight through the air. *Sports Engineering*, 5(4):193–200, nov 2002.

[29] K Bray and D Kerwin. Modelling the Flight of a Soccer Ball in a Direct Free Kick. *Journal of Sports Sciences*, 21:75–85, 2003.

[30] Brandon G Cook and John Eric Goff. Parameter space for successful soccer kicks. *European Journal of Physics*, 27(4):865, 2006.

[31] J. E. Goff, T. Asai, and S. Hong. A comparison of Jabulani and Brazuca non-spin aerodynamics. *Proceedings of the Institution of Mechanical Engineers, Part P: Journal of Sports Engineering and Technology*, 228(3):188–194, 2014.

[32] John Eric Goff and Matt J. Carré. Trajectory analysis of a soccer ball. *American Journal of Physics*, 77(11):1020, 2009.

[33] John Eric Goff and Matt J Carré. Soccer ball lift coefficients via trajectory analysis. *European Journal of Physics*, 31(4):775–784, jul 2010.

[34] Zhengyou Zhang and One Microsoft Way. Flexible camera calibration by viewing a plane from unknown orientations. *Proceedings of the Seventh IEEE International Conference on Computer Vision*, 00(c):666–673 vol.1, 1999.

[35] K Strobl, W Sepp, S Fuchs, C Paredes, and K Arbter. Camera Calibration Toolbox for Matlab, 2009.

[36] S. R Goodwill. Check3D - camera calibration tool for 3D analysis, 2013.

[37] F M White. *Fluid Mechanics*. McGraw-Hill, 7th edition, 2011.

[38] S J Quintavalla. Golf Ball Performance Evaluation Using High-Volume Indoor Aerodynamic Testing. *ITEA Journal*, 22(4):21–25, 2002.

[39] Sadatoshi Taneda. Negative magnus effect. *Reports of Research Institute for Applied Mechanics*, (20), 1957.

[40] Jooha Kim, Haecheon Choi, Hyungmin Park, and Jung Yul Yoo. Inverse magnus effect on a rotating sphere: when and why. *Journal of Fluid Mechanics*, 754, Sep 2014.

[41] Masaya Muto, Hiroaki Watanabe, Makoto Tsubokura, and Nobuyuki Oshima. Negative magnus effect on a rotating sphere at around the critical reynolds number. *Journal of Physics: Conference Series*, 318(3):032021, 2011.